Z. Phys. C - Particles and Fields 26, 199–207 (1984)

Zeitschrift für Physik C Particles and Fields

Pion Pair Production in Photon-Photon Interactions

PLUTO Collaboration

Ch. Berger, A. Deuter, H. Genzel, W. Lackas, J. Pielorz[a], F. Raupach[b], and W. Wagner[c]

I. Physikalisches Institut der RWTH Aachen[d], D-5100 Aachen, Federal Republic of Germany

A. Klovning and E. Lillestöl

University of Bergen[e], N-5014 Bergen, Norway

J. Bürger, L. Criegee, F. Ferrarotto[f], G. Franke, M. Gaspero[f], Ch. Gerke[g], G. Knies, B. Lewendel, J. Meyer, U. Michelsen, K.H. Pape, B. Stella[f], U. Timm, G.G. Winter, M. Zachara[h], and W. Zimmermann

Deutsches Elektronen-Synchrotron (DESY), Hamburg, D-2000 Hamburg 52, Federal Republic of Germany

P.J. Bussey, S.L. Cartwright[i], J.B. Dainton, B.T. King, C. Raine, J.M. Scarr, I.O. Skillicorn, K.M. Smith, and J.C. Thomson

University of Glasgow[j], United Kingdom

O. Achterberg[k], V. Blobel, D. Burkart, K. Diehlmann, M. Feindt, H. Kapitza, B. Koppitz, M. Krüger[l], M. Poppe, H. Spitzer, and R. van Staa

II. Institut für Experimentalphysik der Universität Hamburg[d], D-2000 Hamburg 50, Federal Republic of Germany

Received 14 August 1984

C.Y. Chang, R.G. Glasser, R.G. Kellogg, S.J. Maxfield, R.O. Polvado[m], B. Sechi-Zorn, J.A. Skard, A. Skuja, A.J. Tylka, G.E. Welch, and G.T. Zorn

University of Maryland[n], USA

F. Almeida[o], A. Bäcker, F. Barreiro, S. Brandt, K. Derikum[p], C. Grupen, H.J. Meyer, H. Müller, B. Neumann, M. Rost, K. Stupperich, and G. Zech

Universität-Gesamthochschule Siegen[d], D-5900 Siegen, Federal Republic of Germany

G. Alexander, G. Bella, Y. Gnat, and J. Grunhaus

University of Tel-Aviv[q], Tel-Aviv, Israel

H. Junge, K. Kraski, C. Maxeiner, H. Maxeiner, H. Meyer, and D. Schmidt

Universität-Gesamthochschule Wuppertal[d], D-5600 Wuppertal, Federal Republic of Germany

Abstract. The process $\gamma\gamma \to \pi^+\pi^-$ has been measured with complete particle identification. Cross-sections are presented from near threshold up to the region of the $f(1270)$. In the mass range 0.5–0.7 GeV, cross-sections are lower than the Born term predictions and show no evidence for an $\varepsilon(600)$. The two-photon

[a] Deceased
[b] Now at Université de Paris-Sud, F-91405 Orsay, France
[c] Now at University of California at Davis, Davis, California, USA
[d] Supported by the BMFT, Federal Republic of Germany
[e] Partially supported by Norwegian Council for Science and Humanities
[f] Rome University, partially supported by I.N.F.N., Sezione di Roma, Italy
[g] Now at CERN, CH-1211 Geneva 23, Switzerland
[h] Institute of Nuclear Physics, Ul. Kawiory 26a, PL-30055 Cracow, Poland
[i] Now at Rutherford Appleton Laboratory, Chilton, U.K.
[j] Supported by the U.K. Science and Engineering Research Council
[k] Now at Texaco Europe Computer Information Systems, D-2000 Hamburg, Federal Republic of Germany
[l] Now at Universität Karlsruhe, D-7500 Karlsruhe, Federal Republic of Germany
[m] Now at Northeastern University, Boston, Massachussetts, USA
[n] Partially supported by the Department of Energy, USA
[o] On leave of absence from Instituto de Fisica, Universidad Federal do Rio de Janeiro, Cidade Universitaria, 21910-Ilka do Fundao, RJ, Brasil
[p] Now at BESSY, D-1000 Berlin, Germany
[q] Partially supported by the Israeli Academy of Sciences and Humanities - Basic Research Foundation

width of the $f(1270)$ is found to be in agreement with previous results.

1. Introduction

The reaction $\gamma\gamma \to \pi^+\pi^-$ occurs by means of virtual photons in the process $e^+e^- \to e^+e^-\pi^+\pi^-$. The $\pi^+\pi^-$ mass spectrum can be divided into three regions showing different physical features. Below 1 GeV is a continuum about which little information has hitherto been available; it is of interest to study this region to find out whether it is well described by the Born term and to look for evidence of the suggested $\varepsilon(600)$ state [1]. Between 1 GeV and 1.5 GeV the cross-sections are dominated by the $f(1270)$ resonance, whose shape is affected by interference with a non-resonant background. This region has received extensive study in recent years [2–8]. At higher masses, QCD predictions have been tested [8, 9].

All the previously published measurements of this process [1–9] have been carried out using wide-angle central detectors in e^+e^- storage rings. An important experimental problem is the separation of the $\pi^+\pi^-$ cross-section from that of the kinematically similar electromagnetic processes $\gamma\gamma \to \mu^+\mu^-$ and $\gamma\gamma \to e^+e^-$, which in the absence of particle identification form a background to the $\pi^+\pi^-$ channel. In the region of the $f(1270)$, the cross-section $\sigma_{\gamma\gamma\to\pi\pi}$ is relatively large, and a simple subtraction of a calculated background is possible. At lower masses, however, this background becomes large compared with the $\pi\pi$ signal. The range of measurable $\pi^+\pi^-$ masses is also restricted by the technical difficulties of operating a trigger on low-mass two-track events in central detectors.

The PLUTO experiment at PETRA took data during 1981–82 equipped with forward spectrometers, which have enabled the measured $\pi\pi$ mass range to be extended down to low values. By positively identifying electrons and muons in the forward spectrometer system, it has been possible to recognise $\pi^+\pi^-$ events individually as those not identified as $\mu^+\mu^-$ or e^+e^- events. The need to subtract out a large calculated background is thus avoided. Such an approach is made possible by the fact that particle pairs in a forward spectrometer have a large Lorentz boost relative to the laboratory frame. This gives the produced particles enough energy to make their identification straightforward. Thus, even at invariant masses as low as a few hundred MeV, there is a reasonable probability for at least one of a pair of muons to have enough energy (e.g. $\gtrsim 1$ GeV) to enable it to penetrate an iron filter and be identified. Electrons and positrons can be distinguished from pions at these energies by the amount of energy which they deposit in a shower counter.

In this paper we present the first measurements of $\sigma_{\gamma\gamma\to\pi\pi}$ to extend over a mass range from close to threshold up to the $f(1270)$ region. The two-photon width $\Gamma_{\gamma\gamma}$ of the $f(1270)$ is measured and compared with previous experiments. The cross-sections obtained at lower masses are compared with predictions based on the Born model. Our study is confined to $\pi\pi$ events produced by quasi-real photons, i.e. close to the mass shell, since the limited cross-section for generating highly virtual photons prevented a useful sample of tagged $\pi\pi$ events from being obtained.

2. Apparatus

The PLUTO detector consisted of a cylindrical inner detector surrounded by a cylindrical lead-scintillator shower counter array (the "barrel counter"), and disc-shaped lead-scintillator arrays (the end caps) at the ends. Further details of these items can be found elsewhere [10]. The forward spectrometers were mounted symmetrically at either end of the

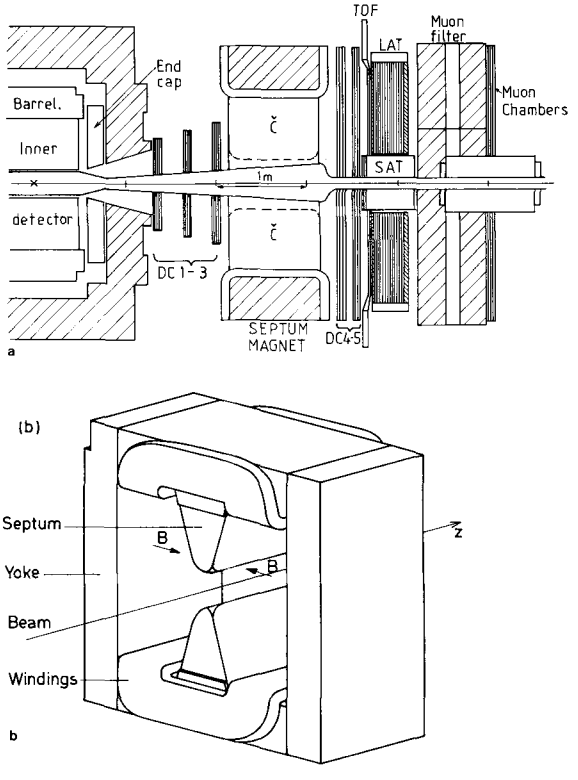

Fig. 1a and b. The PLUTO forward spectrometers: **a** side view of one half of the system, **b** perspective view of a septum magnet. (B = orientation of magnetic field)

main detector, as illustrated in Fig. 1a. Each consisted of the following components.

2.1. Septum Magnets

Each of the two septum magnets (Fig. 1b) consisted of a rectangular iron yoke with two vertical septa. The windings were at the top and bottom of the yoke. The septa thus divided each forward spectrometer into two halves. Particles traversing the spectrometers encountered approximately 0.2 Tesla metres of horizontal magnetic field.

2.2. Drift Chambers

The particle trajectories were measured before and after passing through the magnets by a set of drift chamber modules DC1-DC5. DC1-DC3 each consisted of two sets of two staggered planes which measured the vertical and horizontal co-ordinates, and one plane of wires at 45° to the vertical which was used for pattern recognition purposes only. DC4 and DC5 each contained two staggered planes which measured the vertical co-ordinate; DC4 also contained one plane each of vertical and 45° wires without TDCs, which were used to aid pattern recognition. All wire spacings were 10 mm. The measurement accuracy from a single plane was 0.5 mm, giving an average error on the reconstructed track momentum p of $\pm 0.03\,\mathrm{GeV}^{-1}\ p^2$. Systematic errors on the track momenta were about half this figure. The drift chamber system accepted tracks at angles between 90 and 270 mrad with respect to the beam line.

2.3. Time-of-Flight Counters

Time-of-flight measurement was made by means of scintillation counters situated behind DC5, at 3.6 m from the interaction point. A resolution of ± 0.3 ns was obtained, allowing pion-proton separation up to momenta of 3 GeV/c.

2.4. Large Angle Tagger (LAT)

The LAT was a lead-scintillator shower counter of thickness 14 radiation lengths, covering the angular acceptance of the forward spectrometer. The primary purpose of the LAT was to measure the energies of wide-angle scattered electrons associated with two-photon processes at large values of Q^2, the square of the virtual photon mass. At its centre was a hole which was occupied by the beam pipe and the small angle tagger (see below). Two planes of brass proportional tubes, of width 10 mm and at a depth of 2.5 radiation lengths in the LAT, measured the horizontal and vertical co-ordinates of the showers. The energy resolution of the LAT for photons and electrons was measured by means of Bhabha events to be $\sigma(E)/E = 0.25\,\mathrm{GeV}^{1/2}/\sqrt{E}$. Thus for electrons above 4 GeV in momentum, the momentum resolution of the LAT was superior to that of the drift chamber system.

2.5. Small Angle Tagger (SAT)

The small angle tagger detected electrons and photons at angles in the range 28 to 58 mrad relative to the beam line. It consisted of a circular lead-scintillator array surrounding the beam-pipe, divided into twelve wedge-shaped sectors each with a thickness of 19.3 radiation lengths. The signal from the scintillators was taken out at the inner and outer edges using wavelength shifter bars (BBQ). The outer signal was found to be independent of the impact position and was therefore used to determine the shower energy; the inner signal was position-sensitive and was used to obtain an estimate of the radial position of the shower. Two planes of proportional tube chambers located just in front of the SAT gave a further position measurement for electrons. The azimuthal position was estimated from energy sharing between adjacent sectors. The overall position resolution was approximately ± 1 mrad in polar angle and $\pm 2°$ in azimuthal angle, with an energy resolution of $\sigma/E = 0.17\,\mathrm{GeV}^{1/2}/\sqrt{E}$.

2.6. Čerenkov Counters

The space inside each half of the septum magnets was occupied by a Čerenkov counter containing nitrogen at atmospheric pressure. A signal in this identified a track as an electron. Since the number of Čerenkov photons per track was small, the efficiency for identifying an electron was low (about 50%). However the Čerenkov counters were useful for selecting samples of electron tracks independently of the LAT. The probability for particles other than electrons to be associated with a random Čerenkov hit was about 3%.

2.7. Muon Detection

After traversing the LAT, particles encountered layers of iron of total thickness 0.6 m. This iron, in conjunction with the material in the LAT (0.8 pion interaction lengths), absorbed hadrons, electrons and photons while permitting muons above approximately 1.1 GeV/c in momentum to penetrate to the muon detectors behind. The latter consisted of four

layers of drift chambers mounted on the rear of the iron: two staggered layers with vertical wires and two with horizontal. The drift distance was 80 mm. In practice the drift time information was ignored, since the multiple scattering of muons in the iron made a higher positional accuracy than ± 40 mm unnecessary.

3. Electron and Muon Identification

The present work made use of electron and muon identification to separate events of the type $\gamma\gamma \to \pi^+\pi^-$ from $\gamma\gamma \to \mu^+\mu^-$ and $\gamma\gamma \to e^+e^-$ in the forward spectrometers. The different final states were distinguished as follows:

3.1. e^+e^- Rejection

To identify and eliminate events of the type $\gamma\gamma \to e^+e^-$, the energy E_{LAT} deposited in the LAT was compared with the energy E of the track as measured by the drift chamber system. If the ratio E_{LAT}/E exceeded 0.45 for both particles, the event was classed as an e^+e^- event and was rejected from the final data sample. If one particle missed the LAT or passed through it close to an edge, the event was rejected if the other particle had $E_{\mathrm{LAT}}/E > 0.45$. If neither particle passed through the good region of the LAT, the event was rejected. The limit of 0.45 was established by studying the distribution of E_{LAT}/E in events in which both particles fired the Čerenkov counters in their respective halves of the septum magnet.

These cuts rejected some $\pi\pi$ events, since the pions were measured to have a 15% probability to deposit more than 0.45 of their energy in the LAT. A correction was subsequently applied for this. The contamination of e^+e^- events in the final $\pi\pi$ event sample was estimated from the fraction of events classed as $\pi\pi$ which had hits in both Čerenkov counters. It was found to be negligible ($< 1\%$).

3.2. $\mu^+\mu^-$ Identification

After the rejection of the e^+e^- events, events entering the acceptance of the muon detection system were classed as $\mu\mu$ events if one or both particles gave muon identification, or as $\pi\pi$ events otherwise. For a muon to be identified, a hit was demanded in at least one of the two planes of muon chambers in each orientation, in the region of the track. Corrections for inefficiencies in the muon chambers were found to be small.

To evaluate the correct numbers of $\mu\mu$ and $\pi\pi$ events, it is necessary to know the probability for a given track to give hits in the muon chambers (a) if it is a muon (P_μ), and (b) if it is a pion (P_π). These probabilities were obtained by performing a calculation on each measured track:

(a) To determine P_μ, the multiple scattering, mean energy loss and range straggling in the LAT and iron were calculated from the measured track momentum and its uncertainty. A Monte Carlo procedure then repeatedly generated final track co-ordinates, making a decision as to whether the track would pass through the iron and whether it would end up within the acceptance of the chambers.

(b) Contributions to P_π come from pions simulating muons in three ways: by decaying, by punchthrough and by being associated with noise in the muon chambers. Decay probabilities and angles were generated by the Monte Carlo, and combined with the quantities described above to calculate the probability that a pion could generate a muon chamber hit by decaying. Punchthrough was estimated as in a previous analysis [11]. A map of the noise probabilities over the area of the chamber was constructed by sampling events from the run period, to obtain the probability that a track in any given region of the muon chambers would be associated with noise. Typically, a pion had a probability of 5–10% of simulating a muon, rising to 25% for the highest momentum pions due to their high punchthrough probability. The noise probability was below 1%.

4. Event Selection

The events used in the present analysis were recorded by means of the "forward trigger". Combinations of wires in DC1-DC5 corresponding to tracks originating from the interaction point were stored in a fast memory device, and the wires hit in an event were compared with the stored combinations. In this way possible track candidates were identified. The forward trigger required at least one track candidate in each half of one of the forward spectrometers. (The trigger could not be operated in the other forward spectrometer, owing to severe backgrounds.) Data corresponding to an integrated luminosity $13\,pb^{-1}$ were collected using this trigger.

Events were rejected if there were fewer than two tracks, or if the track configuration in the central detector corresponded to a cosmic ray or to a beam-gas interaction. Clearly identified Bhabha events were removed. Further requirements were now applied to select events of the types $\gamma\gamma \to \mu^+\mu^-$ and $\gamma\gamma \to \pi^+\pi^-$ in the forward spectrometer.

(i) If any charged tracks were found in the inner detector, the event was rejected.

(ii) Two well-reconstructed tracks of opposite charge were required in opposite sides of the triggered forward spectrometer.

(iii) $\gamma\gamma \to e^+e^-$ events were rejected as described in Sect. 3.1.

(iv) The outgoing e^- beam went in the direction of the triggered forward spectrometer, and in a few events the detected negative particle was a scattered beam electron. Events were eliminated if the negative track had $E_{LAT}/E > 0.45$ and a Čerenkov hit. (A correction was made to account for the equal number of such events which lacked a Čerenkov hit owing to the inefficiency of the Čerenkov.)

(v) A high probability for correct muon identification was required. On the hypothesis that a given event was a $\mu\mu$ event, the probability $P_{\mu\mu}$ that it would be identified as such was evaluated from the P_μ values of the tracks. Events were retained only if $P_{\mu\mu}$ exceeded 0.85. This condition was applied to all events, irrespective of whether any muon chamber hits were actually recorded.

(vi) To eliminate backgrounds from other hadronic processes, events with any additional signals in the barrel counter, the end caps, the LATs or the SATs were rejected. This also eliminated tags in the SATs and so ensured that both virtual photons were nearly real.

(vii) At this stage there were 1708 $\pi\pi$ events and 4310 $\mu\mu$ events. The background from beam-gas interactions was now evaluated in the usual way by calculating the position z on the beam axis where each event originated. This was done by taking the track parameters and evaluating z independently for the horizontal and vertical projections of each track. The final z value used was a weighted mean of these four estimates. Figure 2 shows the z distribution for $\pi\pi$ events: a clear peak is seen with little background. The width of ± 25 mm, is greater than the ± 15 mm length of the interaction region by an amount consistent with the measurement errors on the tracks. Events with $|z| > 75$ mm were removed. The background to be subtracted was determined using the wings between $75 < |z| < 225$ mm.

Since the $\mu\mu$ events are about three times as numerous as the $\pi\pi$ events, and each recorded event is assigned to one category or to the other, any error in the $P_{\mu\mu}$ values used will give a correspondingly larger fractional error in the final $\pi\pi$ cross-sections. It is therefore important to verify the calculated P_μ values. This was done by selecting events in which one track was a well-identified muon, and comparing the actual number of events in which the other muon was identified with the predicted number. Corrections were applied to take into account cases where the first track was actually a misidentified pion. The ratio of observed to predicted muon hits was 1.016 ± 0.006, implying a mean systematic error in the final $\pi\pi$ cross-sections of approximately 6% from errors in muon identification. Effects of pion misidentification are also included in this number: a pion giving a false muon chamber hit would not be accompanied by a muon hit from the other track, and this would appear as an apparent inefficiency in the muon detection. The above result thus puts a limit on effects of this kind.

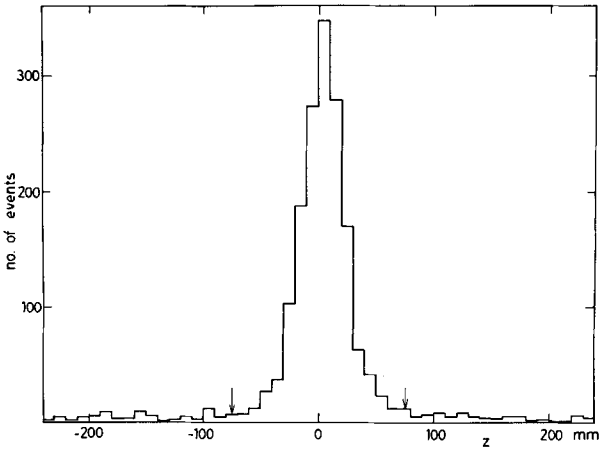

Fig. 2. Reconstructed vertex position z for $\pi\pi$ events

Final checks on the event sample were carried out by examining the time-of-flight spectra for all particles, and the distribution of energies deposited in the LAT by tracks assigned to be muons. In both cases a clean peak was observed around the expected value (i.e. corresponding to light particles and minimum ionising particles, respectively) with negligible background.

5. Data Analysis

5.1. Corrections to the Data

Figure 3 shows the numbers of $\pi\pi$ and $\mu\mu$ events as a function of mass (1) after applying selections (i)–(v), and (2) after further applying selections (vi)–(vii). The cut on z removed about 12% of the $\pi\pi$ events remaining at this stage, predominantly at masses around 0.75 GeV. We attribute this affect to ρ^0 electroproduction off the residual gas in the beam pipe.

It can be seen that selections (vi) and (vii) cause a loss of only about 10% of the $\mu\mu$ events, indicating a generally low level of noise in the photon detectors. About one-third of the original $\pi\pi$ events are eliminated. This indicates a substantial presence of processes giving additional photons in the final

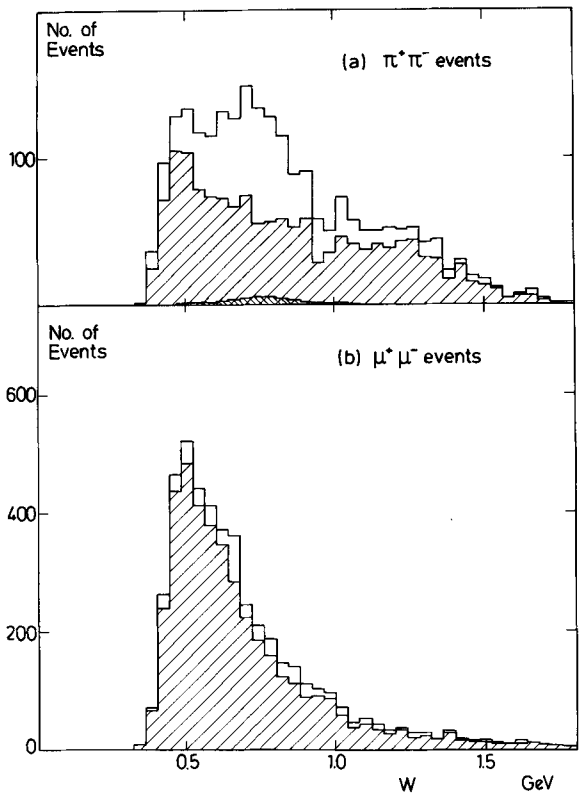

Fig. 3a and b. Distribution of $\pi\pi$ masses **a** for $\pi\pi$ events, **b** for $\mu\mu$ events: (1) after event selections (i)-(v), (2) after additional selections (vi)-(vii) (shaded). In heavy shading is the calculated background from processes having undetected final-state particles

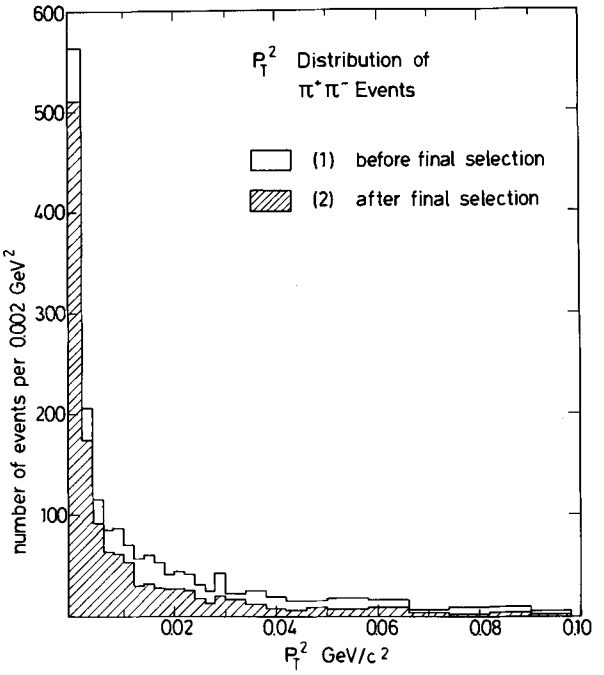

Fig. 4. Distribution in p_T^2 for the $\pi\pi$ events: (1) before, (2) after final event selections as in Fig. 3

state; Monte Carlo studies were therefore performed to estimate the remaining background in the $\pi\pi$ mass spectrum from events with additional undetected particles. The processes considered were $\gamma\gamma \to \eta' \to \rho^0\gamma$, $\gamma\gamma \to \rho^0\rho^0$ and $\gamma\gamma \to A_2 \to \rho\pi$; the cross-sections used in the Monte-Carlo calculations were taken from existing measurements of these channels [12]. The resulting background from these processes is shown in Fig. 3; two-thirds of it is due to the η' process. Backgrounds from other processes giving undetected particles are estimated to be small. That from $\gamma\gamma \to K^+K^-$ was calculated by using the cross-sections from TASSO [13] in a Monte-Carlo calculation which generated K^+K^- events and re-evaluated their apparent cross-section as $\pi^+\pi^-$ events. The K^+K^- background was at most 5% of the $\pi^+\pi^-$ cross-section. It is not included in Fig. 3 but was corrected for in the final results.

Contributions to the observed cross-sections could in principle arise from $\pi^+\pi^-$ pairs produced through virtual bremsstrahlung from the beam electrons. However, such contributions are expected to be small and dominated by ρ-meson production [14], for which there is no evidence in the present results.

Figure 4 shows the p_T^2 distribution of the $\pi\pi$ events before and after event selections (vi) and (vii), where p_T^2 is the square of the overall transverse momentum of the $\pi\pi$ pair. The expected strong peak at low p_T^2 is observed. Contributions to the tail of the distribution come from: events with additional final-state particles, the momentum resolution of the tracks, and the scattering of beam particles through small angles in the two-photon production process (i.e. events with $Q^2 \neq 0$). A comparison between distributions (1) and (2) confirms that the final selections remove a larger fraction of events from the tail than from the peak. No cuts on p_{T^2} were made in the final event sample.

A kinematic fit was made to improve the mass resolution. The overall transverse momentum of the event in the plane of the two tracks was constrained to be zero, with allowance being made for a small contribution of ± 15 MeV/c due to the finite scattering angles of the beam particles.

When plotting the final $\pi\pi$ and $\mu\mu$ mass spectra, weights were included to correct for identification probabilities of less than unity. The numbers of misidentified $\mu\mu$ events were calculated using the $P_{\mu\mu}$ values for identified $\mu\mu$ events, and were subtracted

from the $\pi\pi$ distributions. This correction was large ($\sim 60\%$) at 0.4 GeV, falling to 25% at 0.6 GeV and to below 10% above 0.8 GeV. A corresponding correction for the effects of misidentified pions was applied to the $\mu\mu$ distributions; this correction was $\sim 30\%$ at the $f(1270)$ peak, falling to below 10% at masses less than 1 GeV. At this final stage the backgrounds from beam-gas interactions and final states other than $\pi\pi$ and $\mu\mu$ were subtracted.

5.2. Determination of Cross-Sections

The $\gamma\gamma \to \pi^+\pi^-$ cross-section was evaluated from the ratio of the number of $\pi^+\pi^-$ events to the number of $\mu^+\mu^-$ events in a given mass region. This method is insensitive to uncertainties in the luminosity and the event acceptance, including the efficiencies of the trigger and the track reconstruction. In detail, the method is as follows:

The number of $\pi^+\pi^-$ events recorded in a given interval of W ($\pi\pi$ mass), β (velocity of $\pi\pi$ system relative to lab.) and $\cos\vartheta$ (cosine of $\pi\pi$ decay angle in rest frame, relative to beam axis) can be written as

$$d^3N = N_0(W,\beta)\,A(W,\beta,\cos\vartheta)\frac{d\sigma_{\gamma\gamma\to\pi\pi}(W,\cos\vartheta)}{d\cos\vartheta} \cdot dW\,d\beta\,d\cos\vartheta \qquad (1)$$

N_0 is an overall luminosity factor, and A is the acceptance of the apparatus for $\pi^+\pi^-$ events. A similar expression gives the number of $\mu^+\mu^-$ events in terms of the QED cross section $d\sigma_{\gamma\gamma\to\mu\mu}/d\cos\vartheta$. The quantities β, W and $\cos\vartheta$ for given track parameters are closely similar for $\pi\pi$ and $\mu\mu$ events, owing to the near equality between the π and μ masses. Thus the ratio of $\pi\pi$ to $\mu\mu$ events in a given interval equals the ratio of the cross-sections for the two processes. N_0 and A, since they are the same for both processes, do not need to be known.

The data were treated in the following way. On the basis of the muon identification described above, each event was assigned to either the $\mu\mu$ or the $\pi\pi$ category. The $\mu\mu$ masses were histogrammed with each entry weighted by a factor $(d\sigma_{\gamma\gamma\to\mu\mu}/d\cos\vartheta)^{-1}$ evaluated for the particular event parameters. The various corrections described above were applied, and a smooth curve was fitted to the $\mu\mu$ plot. The $\pi\pi$ mass histogram was finally normalised by the fitted $\mu\mu$ plot, to give the cross-sections for the process $\gamma\gamma \to \pi^+\pi^-$.

This procedure gives values of $d\sigma_{\gamma\gamma\to\pi\pi}/d\cos\vartheta$ averaged over the $\cos\vartheta$ values covered by the experimental acceptance, which are limited to the range $-0.5 < \cos\vartheta < 0.5$. The mean value of $\cos\vartheta$ is zero, with a r.m.s. spread of ± 0.2. Born-term calculations of the process $\gamma\gamma \to \pi^+\pi^-$, and measurements by the CELLO group [7], indicate that the variation in the cross-section over this range of $\cos\vartheta$ can be neglected below the $f(1270)$ mass. This is confirmed by our own results.

In all the above calculations except the evaluation of $d\sigma_{\gamma\gamma\to\mu\mu}/d\cos\vartheta$, the $\mu\mu$ masses were evaluated with the mass of the muon taken as that of the pion. A correction was included to take into account the effect of this approximation on the kinematic and luminosity quantities in Eq. (1). It was typically 5%, rising to 20% at the lowest W values.

As a check, an analysis was performed using only those events in which P_μ was high for both tracks. Muon chamber hits on both tracks were demanded to identify a $\mu\mu$ event. Events with only one muon chamber hit were thus discarded in this analysis. The mean correction to the $\pi\pi$ spectrum from misidentified $\mu\mu$ events was now less than 1%, compared with 10–20% previously. The cross-sections obtained were in agreement with those from the complete data sample.

The range of Q^2 values covered by the experimental acceptance extended from near zero to $-0.25\,\mathrm{GeV}^2$. Both the $\mu\mu$ and $\pi\pi$ Born cross-sections decrease with increasing $|Q^2|$, and possible form-factor effects also alter the $\pi\pi$ cross-section. These factors tend to cancel in the present measurements, however, when the ratio of the $\pi\pi$ to $\mu\mu$ events is taken. The possibility of Q^2-dependent effects was investigated experimentally by performing analyses with cuts imposed on the data at various values of p_T^2. No significant effect was observed. Theoretical calculations indicated that the effect on the measured $\gamma\gamma \to \pi^+\pi^-$ cross-sections should be less than 5% (2% in the $f(1270)$ region). Our conclusion is that the effect of the finite Q^2 range can be neglected in the present work.

6. Results and Discussion

The $\gamma\gamma \to \pi^+\pi^-$ cross-sections are presented in Fig. 5 and Table 1. The points represent the differential cross-section $d\sigma_{\gamma\gamma\to\pi\pi}/d\cos\vartheta$ at $\cos\vartheta = 0$, averaged over the r.m.s. acceptance $d(\cos\vartheta) = \pm 0.2$. Statistical errors only are given; the systematic errors on the cross-sections below 1 GeV are estimated to be approximately 10%, rising to 20% for the four lowest-W points. The cross-sections above 1 GeV are dominated by the $f(1270)$. However, the finite momentum resolution has an important effect even after the kinematic fit, smearing the measured cross-section through $\delta W \approx \pm 60$ MeV at $W = 1$ GeV, with $\delta W \propto W^2$. Thus at the mass of the $f(1270)$, the

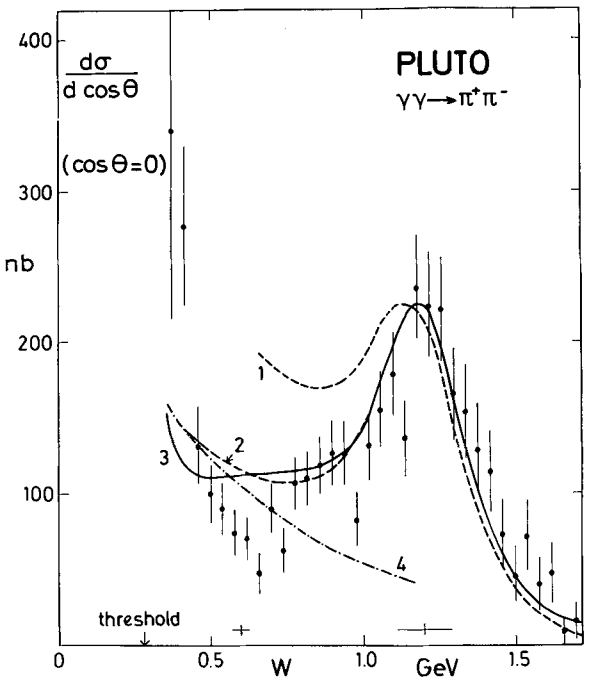

Fig. 5. Differential cross-section for $\gamma\gamma \to \pi^+\pi^-$ at $\cos\vartheta = 0$ as a function of W = measured $\pi^+\pi^-$ mass. Curves 1–3 represent best fits to the data in the $f(1270)$ mass region using (1) Born amplitude + Breit-Wigner with fixed width; (2) Born amplitude + Breit-Wigner (variable width); (3) Mennessier model. Curve 4 represents the conventional Born cross-section alone. Above 1 GeV curve 2 is close to curve 3. The horizontal bars indicate the mean amount of smearing in W at 0.6 GeV and at 1.2 GeV

Table 1. Differential cross-sections for $\gamma\gamma \to \pi^+\pi^-$ at $\cos\vartheta = 0$. The errors are statistical only; systematic errors are discussed in the text

W GeV	$d\sigma/d\cos\vartheta$ nbarn	W GeV	$d\sigma/d\cos\vartheta$ nbarn
0.38	338 ± 125	0.70	89 ± 16
0.42	275 ± 52	0.74	60 ± 15
0.46	130 ± 25	0.78	102 ± 18
0.50	98 ± 19	0.82	104 ± 19
0.54	89 ± 17	0.86	113 ± 19
0.58	73 ± 15	0.90	121 ± 21
0.62	69 ± 14	0.94	122 ± 21
0.66	46 ± 13	0.98	80 ± 18

smearing is of the same order as the $f(1270)$ half-width, and affects its appearance in Fig. 5 considerably. The cross-sections in Table 1 have been restricted to the mass region below 1 GeV. Our data are consistent with the low-statistics results from SPEAR [5] in this lower mass range.

To fit the data to theoretical models, $\mu\mu$ and $\pi\pi$ final states were generated in a Monte Carlo calculation, the $\mu\mu$ state according to the cross-sections of [15] and the $\pi\pi$ according to the models to be investigated. The generated events were passed through a simulation of the forward spectrometer acceptance, and smearing was applied to the momenta of the tracks. Finally the "observed" $\pi\pi$ cross-sections were calculated as in the real data, by normalising the smeared $\pi\pi$ mass distributions to the smeared $\mu\mu$ mass distributions.

The experimental cross-sections were compared with models involving the Born amplitude interfering with the $f(1270)$ described by a Breit-Wigner formula. The Breit-Wigner amplitude for the formation of a spin-2 resonance in photon-photon collisions is given by

$$T = \frac{-5}{2}\sqrt{\frac{M}{W}}\frac{\sqrt{3\Gamma_{\gamma\gamma}\Gamma_{\pi\pi}}}{(W^2 - M^2) + i\Gamma_{\text{tot}}M}\sin^2\vartheta \qquad (2)$$

with the assumption, as in previous experiments, that the $f(1270)$ is produced in a helicity-2 state. Γ_{tot} and $\Gamma_{\pi\pi}$ are the total $f(1270)$ width and the width for $f \to \pi^+\pi^-$ respectively; $\Gamma_{\gamma\gamma}$ is the two-photon width of the $f(1270)$. This amplitude is added to the helicity-2 part of the Born amplitude. The following models were tested:

(i) The simplest possible approach, as used in [5], with constant values for the total and partial widths Γ_{tot} and $\Gamma_{\pi\pi}$. These were taken from the Particle Data Handbook ($\Gamma_{\text{tot}} = 0.18$ GeV; $\Gamma_{\pi\pi} = 0.10$ GeV).

(ii) Mass-dependent widths, with Γ_{tot} and $\Gamma_{\pi\pi}$ varying with W according to the formulae given by Pilkuhn [16], and having the values above at $W = 1.273$ GeV. $\Gamma_{\gamma\gamma}$ was taken to be independent of W. A fixed value for the arbitrary radius r_0 of 1 fm, as used by DELCO [2], was taken.

(iii) The model of Mennessier [1], which makes use of $\pi\pi$ phase shift analyses to parametrise the dynamic properties of the $\pi\pi$ system in terms of poles in the K-matrix. Unitarised amplitudes are calculated. Phase shift solution "C" of [1] was used here (c.f. also [7]) to describe the $\pi\pi$ S-wave, with no direct $\varepsilon(600)$ or $S^*(980)$ contribution.

In all cases, $\Gamma_{\gamma\gamma}$ was varied to fit the data in the mass range 1.0–1.4 GeV around the $f(1270)$ peak. The $f(1270)$ mass M was fixed at 1.273 GeV.

In many situations it is a valid approximation to use a mass-independent resonance width. We see from Fig. 5 that this does not apply, however, in the present case. Model (i) gives an increasingly poor representation of the data as W decreases below the $f(1270)$ resonance region, and will not be considered further here.

Models (ii) and (iii) both give acceptable fits to the data above $W = 0.8$ GeV. Curves 2 and 3 on

Fig. 5 show the respective smeared cross-sections. Below 0.6 GeV the effects of unitarisation become significant; otherwise the two models give similar results. The values of $\Gamma_{\gamma\gamma}$ obtained are 3.25 keV and 2.85 keV for models (ii) and (iii) respectively, with statistical and systematic errors of ± 0.25 and ± 0.5 keV. The latter arises chiefly from uncertainties in the pion punchthrough probabilities in the $f(1270)$ mass region. These values of $\Gamma_{\gamma\gamma}$ are in agreement with previous results, which are mostly in the range 2.5–3.0 keV with systematic errors of typically ± 0.5 keV. The small shift in W in the data points relative to curve 3 is within the range of systematic uncertainties in the mass reconstruction in the forward spectrometer.

Below 0.8 GeV, the data fall below all the theoretical predictions, including also that of Lyth [17]. Between 0.5 and 0.7 GeV the data lie consistently below the Born cross-section alone (curve 4 in Fig. 5), rising above it at the very lowest masses. The results thus confirm that for masses below 1 GeV a mass-dependent $f(1270)$ width (or equivalently, the use of $\pi\pi$ phase shifts) is required, but suggest that alterations to the Born amplitude are also necessary.

It has been proposed that a spin-zero resonance known as the $\varepsilon(600)$ may exist in the $\pi\pi$ system. Our low values of $\sigma_{\gamma\gamma\to\pi\pi}$ in this region provide no evidence for such a state, and exclude a strong coupling of an $\varepsilon(600)$ to the $\gamma\gamma$ system such as suggested in [1]. It should be added that no possibility exists for explaining the low observed cross-sections in terms of destructive interference between an $\varepsilon(600)$ state and the Born amplitude, because the helicity-zero term contributes only about 10% of the Born cross-section in this mass region.

Our results can be summarised as follows:

(i) Below $W=0.8$ GeV, the Born amplitude gives the correct magnitude of cross-section for $\gamma\gamma\to\pi^+\pi^-$ at $\cos\vartheta=0$. However, the W dependence of the cross-section is not well described by the Born amplitude (with or without the addition of an $f(1270)$ term) or by the Mennessier model.

(ii) The $\gamma\gamma\to\pi^+\pi^-$ cross-section above 0.8 GeV is well described by a superposition of the Born amplitude and a Breit-Wigner amplitude for the $f(1270)$, and also by the Mennessier model.

(iii) Using the Mennessier model, the two-photon width $\Gamma_{\gamma\gamma}$ of the $f(1270)$ is found to be $2.85\pm 0.25\pm 0.5$ keV, in agreement with other experiments.

(iv) We see no evidence for production of an $\varepsilon(600)$ in the process $\gamma\gamma\to\pi^+\pi^-$.

Acknowledgements. We wish to thank G. Mennessier and O. Hamon for making available a program to calculate the cross-sections of [1]. We are indebted to the PETRA machine group and the DESY computer centre for the excellent service provided during the experiment. We gratefully acknowledge the efforts of all the engineers and technicians from the various participating institutions who took part in the construction and maintenance of the apparatus.

References

1. G. Mennessier: Z. Phys. C - Particles and Fields **16**, 241 (1983)
2. DELCO Collaboration, A. Courau et al.: Phys. Lett. (to be published)
3. PLUTO Collaboration, Ch. Berger et al.: Phys. Lett. **94B**, 254 (1980)
4. DCI Collaboration, A. Courau et al.: Phys. Lett. **96B**, 402 (1980)
5. MARK II Collaboration, A. Roussarie et al.: Phys. Lett. **105B**, 304 (1981)
6. TASSO Collaboration, R. Brandelik et al.: Z. Phys. C - Particles and Fields **10**, 117 (1981)
7. CELLO Collaboration, H.-J. Behrend et al.: Z. Phys. C - Particles and Fields **23**, 223 (1984)
8. MARK II Collaboration, J.R. Smith et al.: Phys. Rev. D (to be published)
9. PLUTO Collaboration, Ch. Berger et al.: Phys. Lett. **137B**, 267 (1984)
10. L. Criegee, G. Knies: Phys. Rep. **83**, 153 (1982)
11. PLUTO Collaboration, Ch. Berger et al.: Phys. Rev. Lett. **45**, 1533 (1980)
12. J.B. Dainton: Proc. Int. Europhys. Conf. on High Energy Physics, Brighton, 1983, eds. J. Guy, C. Costam
13. TASSO Collaboration, M. Althoff et al.: Phys. Lett. **121B**, 216 (1983)
14. R.M. Godbole, J. Smith: Nucl. Phys. **B158**, 234 (1979)
15. R. Bhattacharya et al.: Phys. Rev. **D15**, 3267 (1977)
16. H. Pilkuhn: Relativistic particle physics. In: Texts and Monographs in Physics, Sect. 4.9 and Appendix A1. Berlin, Heidelberg, New York: Springer 1979
17. D. Lyth: J. Phys. **G10**, 39 (1984)